REVEALING MARS' MANTLE PLUMES USING WRINKLE RIDGE GEOMETRIES

C. B. Beddingfield[1], J. E. Moersch[1], H. Y. McSween[1], [1]Department of Earth and Planetary Sciences, University of Tennessee, Knoxville, TN, USA (cbeddin1@vols.utk.edu).

Introduction: The presence of Tharsis and Elysium suggests that Mars' mantle contained two large upwelling plumes that were active during the Early Hesperian [e.g., 1, 2]. Although the presence of Tharsis and Elysium is most consistent with a two-plume mantle model, it is also possible that additional smaller plumes, that did not manifest on the surface, existed in these regions based on numerical modeling results [e.g., 2, 3, 4, 5]. The sizes and number of plumes is largely dependent on mantle temperature [6], phase transitions, and the size of the martian core [e.g., 7, 8, 9]. This information would provide insight into a martian fluid core [10] and magnetic field [11].

The presence of additional plumes could be revealed by variations in surface heat fluxes. In general, lower heat fluxes are present above the edges of upwelling plumes and higher heat fluxes are present above the plume centers [2]. Local vertical thermal gradients and surface heat fluxes can be estimated if the local brittle-ductile transition (BDT) depths can be constrained [e.g., 12, 13, 14].

Wrinkle ridges are surface folds that consist of underlying thrust faults [e.g., 12, 15] that likely interacted with the BDT at depth during their formation. This interpretation is based on their large lengths, which are up to several hundreds of kilometers [e.g., 12, 15, 16]. Because these faults interacted with the BDT, they are likely listric in geometry [17, 18, 19], meaning that they are concave-up faults that decrease in dip with increased depth and eventually transition into the sub-horizontal BDT. The BDT depth affects the thickness of the deformed layer, which affects fault geometry (Figure 1a). Therefore, the surface manifestations of listric thrust faults can be used to constrain the local BDT depths [20], and therefore surface heat fluxes.

Data Collection: A system of abundant sub-parallel wrinkle ridges formed circumferential to Tharsis in response to lithospheric loading from the development of the Tharsis Rise during the Early Hesperian [e.g., 16, 21, 22]. We focus on circum-Tharsis wrinkle ridges in the northern lowlands because these ridges are pervasive, Early Hesperian in age, and the region is otherwise flat over large scales [16, 23, 24], allowing for more accurate geometric measurements.

We measure wrinkle ridge geometries using images taken by the Context Camera (CTX) onboard the Mars Reconnaissance Orbiter (MRO) and elevation point data taken from the Mars Orbiter Laser Altimeter (MOLA) onboard the Mars Global Surveyor (MGS) spacecraft. CTX images that overlie each wrinkle ridge sample location were processed and map-projected using the Integrated Software for Imagers and Spectrometers 3 (ISIS 3) [25]. The MOLA point data overlying each sample location were collected. These images and data were exported to ArcMap for measurements and analyses. In each sample location, we created profile lines across the associated wrinkle ridge. Measurements will be taken along each profile line to statistically compare heat flux calculation results.

Methods: We are using various measurements of wrinkle ridge geometries to estimate the depth to the BDT and the surface heat flux in the region of each wrinkle ridge (Figure 1). As discussed in [20], when a fault is listric and interacts with the BDT at depth, that depth is given by

$$d = \left(\frac{W_m + H}{\sin\theta}\right)[\cos(\theta - \phi) - \cos\theta], \quad (1)$$

where W_m is the tilted back limb width of the wrinkle ridge and ϕ is the difference between the maximum and minimum dips along the fault, which is equivalent to the value for θ when a fault is listric and transitions into a horizontal detachment at depth. H is the hinge migration, given by

$$H = \frac{W_m}{\left[\left(\frac{\tan\theta}{C}\right) - 1\right]}, \quad (2)$$

θ is the near surface dip of the thrust fault, given by

$$\theta = 45° - \frac{\arctan(\mu)}{2}, \quad (3)$$

and μ is the coefficient of friction. C is defined as

$$C = \sin\alpha - \left(\frac{1 - \cos\alpha}{\tan\alpha}\right), \quad (4)$$

and α is the surface slope of the back limb.

Laboratory experiments show that μ typically lies in the range of 0.5–1.0 for rocks, and these values are correlated with θ values that range from 23° - 32° when formed in isotropic rock [26] (Equation 3).

The temperature at the BDT can be found by equating the brittle and ductile strengths of a material and solving for temperature. We take the scheme for calculating heat flux at the time of faulting from [27] and [28]. The brittle strength of a material under pure compression, (σ_1-σ_3), is given by

$$(\sigma_1 - \sigma_3)_b = K\rho g d \quad (5)$$

where K is the coefficient depending on the stress regime, and is equal to 3 in the case of pure compression [e.g., 29, 30], ρ is material density, and g is the gravitational acceleration of Mars, which is 3.72 m s^{-2}.

The ductile strength of rock under compression is given by

$$(\sigma_1 - \sigma_3)_d = \left(\frac{\dot{e}}{A}\right)^{\frac{1}{n}} \exp\left(\frac{Q}{nRT}\right) \quad (6)$$

where $\dot{e}$ is strain rate, A and n are empirical constants, Q is the activation energy of creep, R is the gas constant, equal to 8.31474 J mol^{-1} K^{-1}, and T is the temperature. We use strain rates, $\dot{e}$, ranging from 10^{-16} s^{-1} and 10^{-19} s^{-1} based on the range

estimated for Mars [31, 32, 33] and intra-plate strain rates on Earth [34]. We use creep parameters of diabase which is relevant to the Martian crust, which are A=0.0612 MPa^{-n}s^{-1}, n=3.05, and Q=276 kJ mol^{-1} [27, 35].

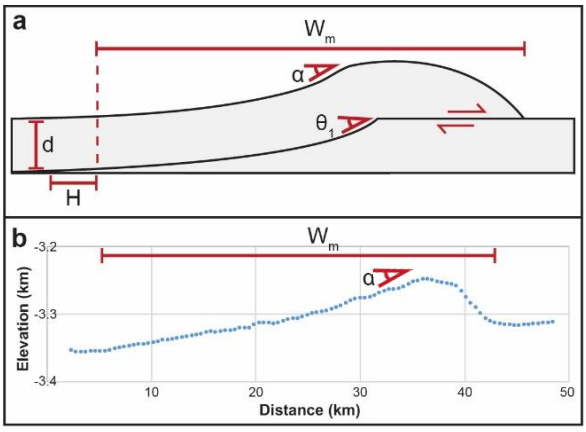

Figure 1: a) Wrinkle ridge diagram. W_m is the tilted back limb width of the wrinkle ridge, α is the slope of the back limb, θ is the near surface dip, H is the hinge migration, and d is the depth to the BDT. b) Example of how measurements will be taken of wrinkle ridge topography.

The temperature at the BDT is expressed where

$$T_d = \frac{Q}{R}\left[\ln \frac{AK\rho g d}{\dot{e}}\right]^{-1} \quad (7)$$

and the thermal gradient is given by

$$\Delta T = (T_d - T_s)/d \quad (8)$$

where T_d is temperature at the BDT and T_s is surface temperature. The present mean temperature at the surface of Mars is 220 K [36]. The BDT depth, d, determined from Equation 1 that depends on the geometric variables measured during characterization of a wrinkle ridge is substituted into Equation 7 to yield a heat flux value. From the thermal gradient, the surface heat flux is given by

$$F = \frac{k_c(\Delta T)}{d} + \frac{dh}{2} \quad (9)$$

where k_c is the thermal conductivity of the crust and is estimated to be 2 W m^{-1} K^{-1} for Mars [37]. The volumetric heat production rate, h, from the martian crust is estimated to be between 0.46 and 0.60 μW m^{-3} [27]. Using these equations, we will estimate and map martian heat fluxes, where circum-Tharsis wrinkle ridges are present, across the northern lowlands. The spatial distributions of these heat fluxes will then be analyzed to test for the presence of additional Early Hesperian mantle plumes in this region.

Preliminary Results: Based on our results so far, we have found that the Early Hesperian surface heat fluxes in the northern lowlands near Tharsis are between 50 and 80 mW m^{-2}. This result is consistent with other Early Hesperian heat flux values calculated using different techniques. For comparison, a Hesperian heat flux of 54-66 mW m^{-2} was calculated in the region of Coracis Fossae in the southern highlands [38]. However, some heat flux estimates in other regions of Mars are lower. For example, heat fluxes of 22-47 mW m^{-2} and 31-49 mW m^{-2} were estimated for the Solis Planum region [39] and Amenthes region [27], respectively. Once all other heat flux values are calculated within each sample location in our study areas, additional comparisons of these values will be made. Our calculation results for each study area will be analyzed using a set of statistical tests.

If the two-plume model is best characterizing of the Early Hesperian martian mantle, and no other mantle plumes were present in the vicinity at the time, then the heat flux would have been progressively lower with distance from Tharsis. This pattern reflects the decrease in plume temperature away from the plume center. However, if multiple plumes existed in this region, there should either be a weak correlation or no correlation between heat fluxes and distance from Tharsis. To test for a negative correlation, we will conduct a regression analysis using the R software.

Discussion: The results of this work will provide important constraints on the history of Mars' mantle and thermal structure. For example, the number and geometry of plumes within the martian mantle is strongly influenced by the mode of heating [5]. As summarized in [5], if Mars' mantle consists of a small number of plumes, then the mantle is likely hot, with a large amount of heat being transferred from the core. However, if Mars' mantle consists of more than two plumes, then less heat is transferred from the core and the mantle is likely cooler. The results from this work will have implications for Mars' mantle plume structure, the amount of heating provided to the mantle from the core, core size, and will provide information important for investigating the existence and lifespan of a fluid core and magnetic field. Additionally, this work provides a new technique for calculating heat fluxes on Mars that can also be used on other planetary bodies including Mercury, Venus, and the Moon.

References: [1] Schubert et al. (1990) [2] Li and Kiefer (2007) [3] Lingenfelter and Schubert (1973) [4] Zaranek and Manga (2007) [5] Schubert et al. (2001) [6] Olson et al. (1987) [7] Schubert et al., (1995) [8] Harder and Christensen (1996) [9] Harder (1998) [10] Yoder et al. (2003) [11] Acuña et al. (2001) [12] Golombek et al. (1990) [13] Tate, 2002 [14] Okubo and Schultz (2003) [15] Golombek et al. (2001) [16] Head et al. (2002) [17] Jackson and McKenzie (1983) [18] Shelton (1984) [19] Brune and Ellis (1997) [20] Amos et al. (2007) [21] Banerdt et al. (1992) [22] Watters and Maxwell (1986) [23] Smith et al. (1998) [24] Kreslavsky and Head (2000) [25] Anderson et al. (2004) [26] Anderson (1951) [27] Ruiz et al. (2008) [28] Ruiz et al. (2011) [29] Sibson (1974) [30] Ranalli (1997) [31] McGovern et al. (2002) [32] McGovern et al. (2004) [33] Schultz (2003) [34] Tesauro et al. (2007) [35] Caristan (1982) [36] Kieffer et al. (1977) [37] Clifford (1993) [38] Grott et al. (2005) [39] Ruiz et al. (2006)